Elliptically Bent X-ray Mirrors with Active Temperature Stabilization

Sheng Yuan,[1] Matthew Church,[1] Valeriy V. Yashchuk,[1] Kenneth A. Goldberg,[2] Richard S. Celestre,[1] Wayne R. McKinney,[1] Jonathan Kirschman,[1,*] Gregory Morrison,[1] Tino Noll,[3] Tony Warwick,[1] Howard A. Padmore[1]

[1]*Advanced Light Source, Lawrence Berkeley National Laboratory, Berkeley, CA 94720, USA*

[2]*Center for X-ray Optics, Lawrence Berkeley National Laboratory, Berkeley, CA 94720, USA*

[3]*Helmholtz Zentrum Berlin für Materialien und Energie, Elektronenspeicherring BESSY-II, Albert-Einstein-Str. 15, 12489 Berlin, Germany*

Abstract. We present details of design of elliptically bent Kirkpatrick-Baez mirrors developed and successfully used at the Advanced Light Source for submicron focusing. A distinctive feature of the mirror design is an active temperature stabilization based on a Peltier element attached directly to the mirror body. The design and materials have been carefully optimized to provide high heat conductance between the mirror body and substrate. We describe the experimental procedures used when assembling and precisely shaping the mirrors, with special attention paid to laboratory testing of the mirror-temperature stabilization. For this purpose, the temperature dependence of the surface slope profile of a specially fabricated test mirror placed inside a temperature-controlled container was measured. We demonstrate that with active mirror-temperature stabilization, a change of the surrounding temperature by more than 3K does not noticeably affect the mirror figure. Without temperature stabilization, the surface slope changes by approximately 1.5 µrad rms (primarily defocus) under the same conditions.

* Now at Ikawamachi Board of Education, Minamiakitagun, Akitaken 018-1516, Japan.

1. Introduction

Beamlines at third- and fourth-generation synchrotron radiation light sources achieve unprecedented high-brightness and low emittance, producing coherent x-ray beams that demand x-ray optics suitable for micro- and nano-focusing and brightness preservation. The required quality of the corresponding reflecting optics is characterized with root-mean-square (rms) slope error tolerances below 0.3 µrad with significantly curved and sophisticated surface shapes [1,2].

One of the most effective and widely used ways to achieve precise focusing is to use two, orthogonal, elliptically cylindrical reflecting elements at glancing incidence, the so-called Kirkpatrick-Baez (KB) pair [3], which focuses the beam separately in the tangential and sagittal directions. Recently, significant progress in the direct fabrication of elliptical surfaces has been achieved [4-6]. However, the cost of directly fabricated tangential elliptical cylinders is often prohibitive. This is in contrast to flat optics, which are simpler to manufacture and easier to measure by conventional surface profilometry. In order to get the desired surface figure, a flat substrate, appropriately shaped in the sagittal direction, is precisely bent by applying torques (couples) at each end [7]. Besides the cost efficiency, bendable reflecting optics are free of chromatic aberration, amenable to tuning, and useful for adaptive (active feedback) applications. In addition, bendable optics give us the flexibility to leave the sample fixed and to adjust the focus into the correct position.

The manufacture and use of high quality x-ray optics requires surface metrology with an accuracy of better than 0.1 µrad [8]. While the accuracy of ex situ x-ray mirror metrology

and tuning techniques has improved over time [9-15], the performance of optics on beamlines is still limited by environmental factors specific to their beamline applications [16-19]. Indeed, at beamlines, variations of the ambient temperature, vibration, temperature gradients due to x-ray absorption on the mirror's substrate, etc., are significantly different from that in an optical metrology lab. These factors require sophisticated environmental control of optical systems [20-22] and high-accuracy, at-wavelength, in situ metrology techniques for fine tuning and alignment of optics at beamlines [23-29].

For the performance of bendable x-ray optics used for fine focusing at the beamline end-stations, thermal effects that depend on ambient temperature variation are especially troublesome. Mirror shape changes are induced by differences in the thermal expansion coefficients of the various materials used in the mirror-bending holder. In this paper, we present the design and laboratory testing of an elliptically bent KB mirror with active temperature stabilization. Mirrors with a similar design are now successfully used at the Advanced Light Source (ALS) for submicron focusing [30].

2. Mirror design

Figure 1 shows details of the mirror bender design. The bending mechanism of the mirror is based on two cantilever springs. With a wire, each cantilever spring is connected to a displacement-reduction spring that is driven with a Picomotor^{TM}. The displacement of the Picomotor^{TM} actuators is monitored with linear variable differential transformers (LVDT) with an accuracy of approximately 100 nm over the useful range. The bender design allows extremely fine control of the bending couples applied to the mirror substrate.

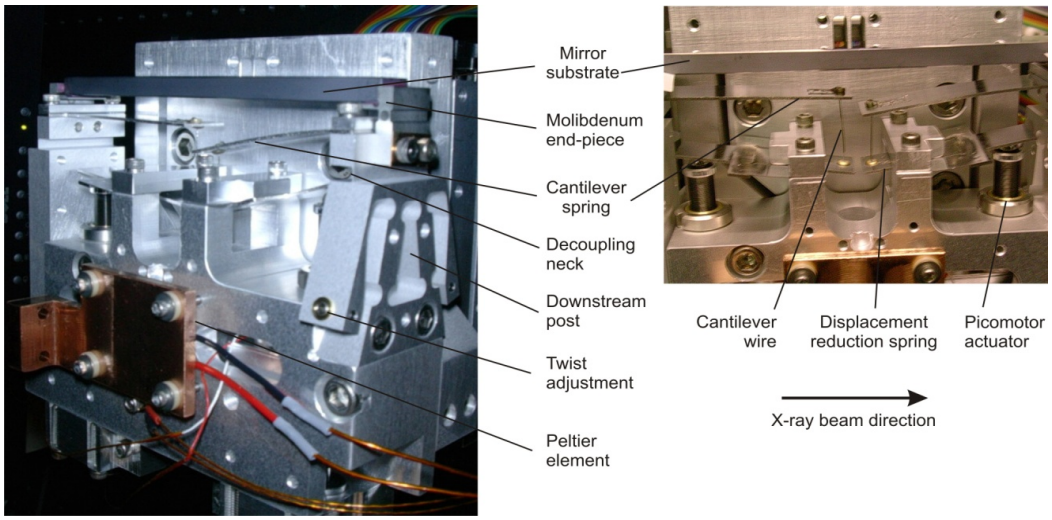

Fig. 1. Bendable KB mirror used for the thermal investigations.

The mirror design and the materials used have been carefully optimized to provide a high heat conductance between the mirror body and the substrate. The mirror body and the most of the elements of the mirror assembly are made of aluminum which reduces the fabrication costs. Molybdenum end-pieces are glued to the silicon mirror substrate. The thermal conductivity of molybdenum (at room temperature) is approximately 138 $Wm^{-1}K^{-1}$, smaller than of aluminum (~237 $Wm^{-1}K^{-1}$) by a factor less than two, and larger than invar (~14 $Wm^{-1}K^{-1}$), which is commonly used in similar applications, by a factor of

approximately ten. The mirror design and the selection of these materials allow efficient temperature stabilization of the mirror with a Peltier element attached directly to body of the mirror assembly (Fig. 1).

The mirror-bender design used in the present work is closely related to the design of KB mirrors fabricated for ALS beamline 12.3.2 [30]. Three similar mirrors are also used for micro-focusing at ALS beamline 10.3.2. In both cases, mirrors with active temperature stabilization based on a Peltier element have shown a significantly better x-ray focusing and stability performance than previous mirrors without temperature stabilization.

In this work we present the results of ex situ visible-light shape measurement tests on a single KB mirror fabricated for use as a test x-ray optic at ALS beamline 5.3.1. The tests were conducted at the ALS Optical Metrology Laboratory (OML). A new endstation on beamline 5.3.1, developed in the course of an LDRD (Laboratory Directed Research and Development Program) project [31,32], is dedicated to the investigation of at-wavelength metrology of x-ray optics. The test mirror substrate and its intended surface profile, when bent, were designed for vertical focusing on ALS beamline 10.3.2, with optical specifications given in Table 1.

Table 1. Original specifications of the KB test mirror.

Substrate material	Substrate thickness	Substrate length	Mirror center radius of curvature	Object distance	Image distance	Grazing angle
Si	5.08 mm	101.6 mm	57.14 m	2400 mm	120 mm	4.0 mrad

3. Assembly, initial alignment and adjustment of the test mirror

The assembly, preliminary alignment, and the setting of the mirror benders are performed by monitoring the mirror surface shape with a 6-inch ZYGO^{TM} GPI interferometer at the OML.

First, with relaxed cantilever springs, the mirror substrate, with glued molybdenum end-blocks, is attached to the bender mechanism (Fig. 1). The downstream post is tightened to the mirror body, while the upstream post is loosened. Final positioning and tightening of the upstream post is made in such a way as to provide the smallest possible curvature of the installed substrate. The upstream post has two decoupling flexures that decrease the parasitic stress applied to the mirror substrate due to assembly error. The downstream post is equipped with an anti-twist mechanism and has one decoupling flexure. The flexures, which are 380 μm thick, do not provide complete stress decoupling apparently due to a small misalignment of the parts and a difference between the length of the substrate and the distance between the posts. The latter perturbation can cause a tension effect [7]. As a result, the mirror's radius of curvature due to residual stress begins at approximately 500 m (concave), with totally released cantilevers.

Second, the twist in the mirror substrate is removed using the dedicated downstream anti-twist adjustment shown in Fig. 1. The anti-twist mechanism is designed with its axis of rotation on the reflecting surface of the mirror. Figure 2 shows normal-incidence interferograms of the mirror surface recorded before and after the twist correction.

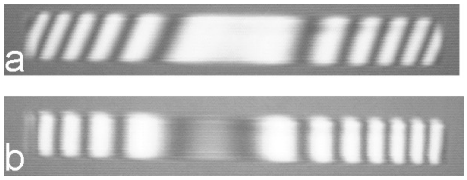

Fig. 2. Mirror twist correction with the ZYGO™ GPI interferometer. The interferograms of the mirror surface before (a) and after (b) the twist correction are shown.

Third, a ZYGO™ GPI interferometer is used to measure the tangential radii of curvature from three sections of the mirror's clear aperture (upstream, central, and downstream). The mirror is iteratively bent to a shape close to the desired ellipse specified in Table 1 based on three local curvature values. The interferometer's measurements over the entire clear aperture of the mirror are limited to a relatively large radius of curvature, above ~200 m. Therefore, its measurements are only used to confirm that the benders have the required range of tuning.

Finally, the anti-twist correction process is repeated for the central part of the bent mirror. Later, a final, more precise anti-twist correction is performed using slope measuring profilers, including the upgraded ALS Long Trace Profiler LTP-II [12] and the Developmental Long Trace Profiler (DLTP) [13], in the ALS OML. In this correction, the sagittal surface slope profile along the entire clear aperture of the mirror is measured; and the sagittal slope variation is minimized by manually tuning the twist adjustment screws (Fig. 1). For illustration, Fig. 3 shows the sagittal slope profiles of the mirror measured before and after twist correction. The twist correction removed a linear part of the sagittal slope variation that initially had peak-to-valley (PV) variation of 63 µrad. After the correction, the residual sagittal slope variation has a quadratic dependence on the tangential position with a PV variation of 24 µrad. We attribute the uncorrected sagittal slope variation to an asymmetrical stress of the substrate due to tolerances of the mirror assembly. Note that at glancing incidence, the effect of sagittal slope errors are reduced, relative to the tangential errors, by a factor that is on the order of the grazing incidence angle. For this reason, sagittal errors of this small magnitude, across the illuminated width of the mirror, will have little impact on focusing performance.

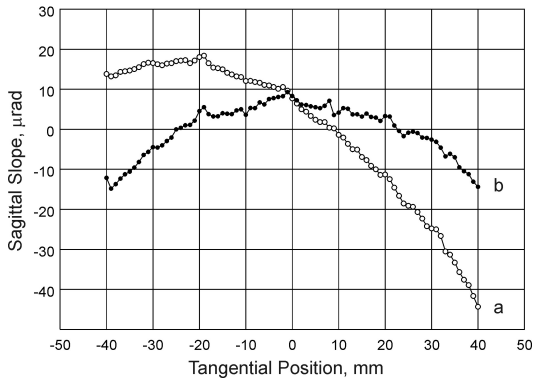

Fig. 3. Mirror twist correction with the DLTP. The sagittal slope profiles of the mirror measured **(a)** before, and **(b)** after twist correction.

Note that when setting a set of KB mirrors for a beamline at the OML, the mutual perpendicularity of the mirror surfaces is aligned using the ZYGO™ GPI interferometer and a 90° optical reference cube.

4. Precision setting and characterization of the mirror benders

For optimally setting the mirror benders with a slope-measuring profiler, the DLTP [12] or the upgraded ALS LTP-II [13], we use an original procedure developed at the OML and described in Refs. [14,15]. The procedure utilizes the near linearity of the bending problem. In this case, the minimum set of data necessary for characterization of one bender consists of three slope traces: (1) an initial measurement, $\alpha_1(x_i)$; (2) measurement after adjustment of the bending couple C_A by ΔC_A, $\alpha_2(x_i)$; and (3) measurement after adjustment of the second bending couple C_B by ΔC_B, performed at C_A, $\alpha_3(x_i)$. These three measurements, and their differences, provide a complete experimental characterization of the mirror benders, using the benders' characteristic functions:

$$f_A(x_i) = [\alpha_2(x_i) - \alpha_1(x_i)]/\Delta C_A \quad \text{and} \tag{1a}$$

$$f_B(x_i) = [\alpha_3(x_i) - \alpha_1(x_i)]/\Delta C_B . \tag{1b}$$

Using a method of linear regression analysis with experimentally found characteristic functions of the benders, a prediction for a slope trace $\alpha_0(x_i)$, which is the best achievable approximation to the desired slope trace, and the corresponding optimal bending couplings, C_A^0 and C_B^0 are calculated. With this method [14,15], the characteristic functions of the benders given by Eqs. (1a) and (1b) can be used for retuning of the optics to a new desired shape without removal from the beamline and ex situ re-measuring with a slope profiler.

Figure 4 shows the characteristic functions of the test mirror, measured with the DLTP. As a measure of the bending couplings C_A and C_B, we use the readings from the LVDT sensors, measuring the displacements of the two Picomotor™ screws in microns. Note that the characteristic function of the upstream bender A (Fig.1) has a higher slope for the region closest to its bender; the opposite (downstream) side of the mirror surface is significantly less sensitive to the change of the bending coupling C_A. Similarly, the downstream bender B produces stronger curvature bending of its adjacent region of the mirror surface.

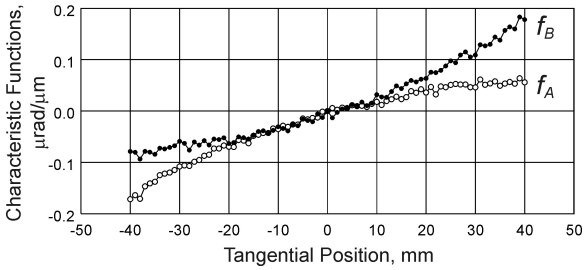

Fig. 4. Characteristic functions of the test mirror benders measured with the DLTP: for the left-hand-side (upstream) bender (f_A) and for the right-hand-side (downstream) bender (f_B).

Once the predicted values of the optimal bending couplings (C_A^0 and C_B^0) are set, the mirror is measured once more to verify its shape. The inherent accuracy of the procedure is limited only by the current accuracy and precision of the OML slope measurements with the LTP-II and DLTP, which are close to 0.1 μrad.

Figure 5 shows the residual variation of the mirror tangential slope and height after subtraction of the desired elliptical shape. The variation, characterized with an rms slope variation of 0.5 μrad, is mostly due to the systematic, fourth-order, "bird-like" residual surface figure, with very little higher spatial frequency variation. There are a few sources potentially contributing to this figure error. As we have mentioned in Sec. 3, the current mirror assembly design does not allow for total compensation of the tension effect [7]. Fabrication errors of the sagittal shape and the thickness of the substrate are also possible.

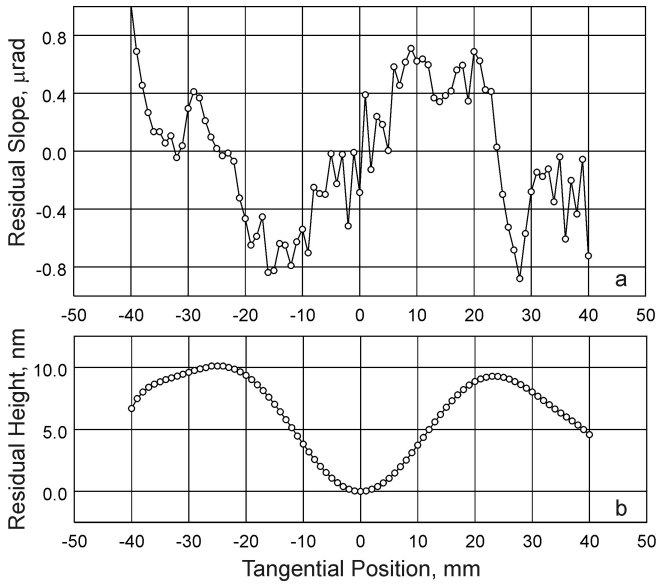

Fig. 5. The residual variation of the mirror tangential slope after subtraction of **(a)** the desired shape. **(b)** The corresponding height trace obtained by a numerical integration of the slope trace.

Note that for the present investigation (unlike a beamline focusing application), the presence of the figure error is even useful for distinguishing a real change of the mirror shape from measurement errors.

From numerical simulations presented elsewhere [32], we also found the image distance may be slightly altered (then the mirror re-bent according to the optimal bending techniques [14,15]) to correct the residual fourth order aberration, thus resulting in a overall better mirror shape.

5. Experimental set up for thermal tests

A special container with variable inside temperature was built for the LTP-II surface profile studies of the thermal dependence of x-ray optics. The container, with the KB mirror assembly inside, and the front side temporarily removed for inspection, is shown in Fig. 6, as it was arranged for LTP-II measurements.

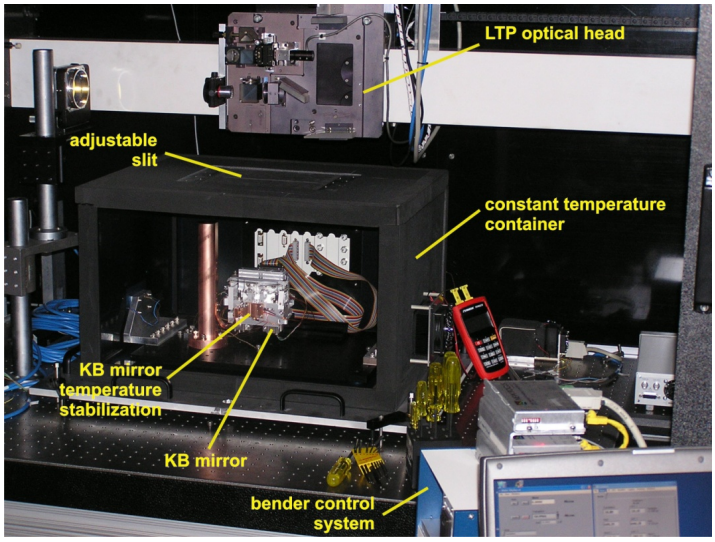

Fig. 6. The container and the experimental arrangement for the LTP investigation of thermal effects with the bendable KB mirror. The mirror faces upward.

The design of the container is based on a standard Thorlabs^{TM} breadboard enclosure with plexiglass walls and feed-through panels on one of the sidewalls. For thermal isolation from the environment, the outside surface of the container is covered with self-adhesive thermal insulation material. The temperature inside the container is controlled with two actively stabilized Peltier elements. A temperature controller is utilized to supply current (5 A maximum) to the Peltier elements, connected in parallel, and to stabilize the temperature inside the container. A temperature transducer AD590, used as a feedback temperature sensor, is mounted on a bracket of one of the Peltier elements. One more temperature sensor, mounted in the center of the container breadboard, is used for monitoring temperature inside the container. A comparison of temperatures measured with the two sensors provides a measure of the temperature gradient. Test experiments with the container found that the uniformity of inside temperature variation is less than 0.3 C when the temperature range is within 4 C of room temperature.

For precise alignment of the upward-facing mirror with respect to the LTP-II light beam, there are four fine height adjusting screws placed at the corners of the container base plate (Fig. 6). The LTP-II scans the mirror surface through an open, 200 mm (length) × 10 mm (width) slit, movable in the sagittal direction.

6. Thermal effect on the mirror surface shape

Mirror shape measurements at different stable, environmental temperatures were made with and without mirror-thermal stabilization.

After setting and characterization with the DLTP, the mirror was placed in the container mounted on the LTP-II optical table. The first set of LTP-II tests with the mirror were to investigate the mirror shape dependence on ambient temperature, without mirror temperature stabilization. Between shape measurements, a one hour time delay was given to reach thermal equilibrium inside the container.

A precise reference measurement at room temperature of 21 C was carried out after re-setting of the mirror shape to the desired ellipse with the LTP. In order to suppress

random noise and the error due to set-up drift, a measurement run consisted of eight sequential scans performed according to the optimal scanning strategy suggested in Ref. [33]. At the best bent shape, the KB mirror's residual rms slope error was 0.55 µrad (Fig. 7). While this is slightly larger than for the optimal bending obtained with the DLTP, the difference may be due to the increased systematic error of the LTP measurements due to the large distance between the LTP optical head and the mirror surface (Fig. 1). See also a relevant discussion in Ref. [12].

Figure 7 summarizes the surface shape measurements performed at different temperatures inside the container, without mirror temperature stabilization. As the temperature within the container increases, the slope error of the originally best bent mirror increases.

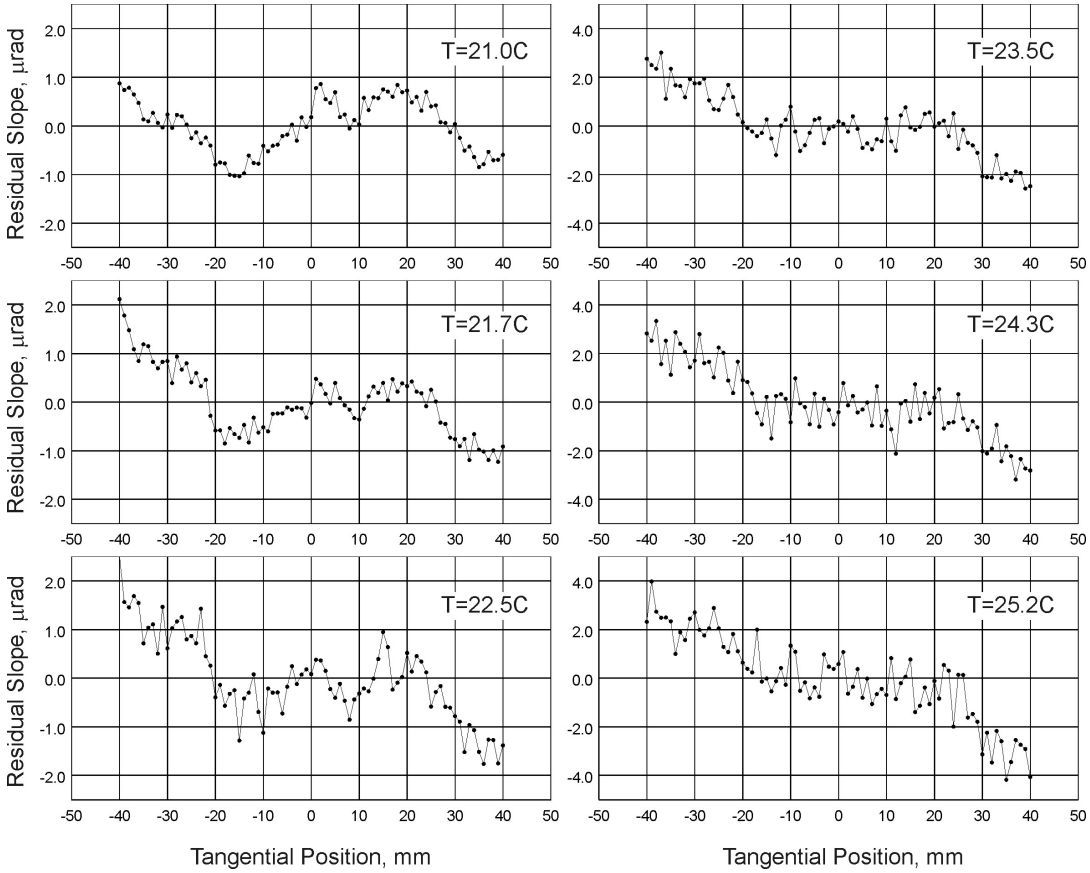

Fig. 7. The residual variation of the mirror tangential slope measured at different temperatures inside the container and at the same setting of the benders. The traces correspond to the sagittal center of the mirror. Note that the vertical range of the plots in the right column is twice of that of the left one.

The primary cause of the increase is the difference of thermal expansion of the mirror holder's aluminum body and the silicon mirror substrate (see Sec. 2). A simple estimation based on 100 mm substrate length gives a thermal expansion difference of 10 µm at $\Delta T = 5$ C. The thermal expansion contributes to the tension the mirror assembly, leading to a change of the mirror shape.

Figure 8 shows the surface slope change due to thermal effects at the extreme temperature of $T = 25.2°C$ (remove the degree symbol, it is redundant, and not SI units)

within the measurement series. The slope change is obtained by subtracting the 21 C reference slope trace from the 25.2 C trace. The mirror slope change from the increased temperature has a linear form (cylindrical shape). Since the surface slope is the first order derivative of the surface height (sag), the linear difference slope term manifests as a focus error that will displace the focus longitudinally or blur the focal spot in a fixed image plane.

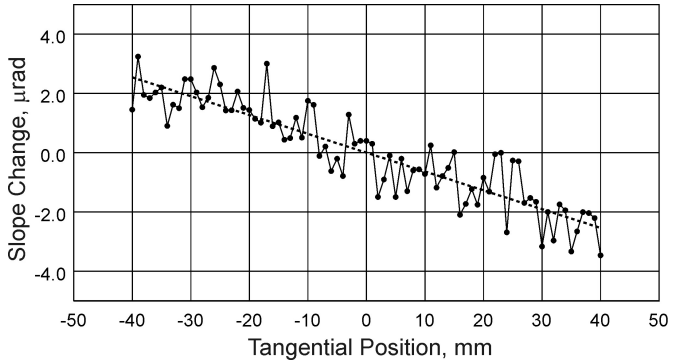

Fig. 8. Temperature-induced surface slope change from a 4.2 C (25.2 C–21.0 C) temperature rise. The linear behavior represents a defocus with an effective convex radius of 15.7 km (dashed line).

The measured curvature changes with changing temperature are given in Table 2. As in Fig. 8, linear fitting to the slope trace differences are used for this measurement. The table also provides the corresponding values of the rms slope variation. To compensate the thermal effects, we can introduce defocus to the focal plane; the corresponding necessary defocus and the RMS slope error after the compensation are listed in Table 2 also.

Table 2. Mirror curvature change and RMS slope error corresponding to different container temperatures, relative to the initial 21 C state. The corresponding focal change and residual RMS slope error (after compensation) are also given.

T [C]	21	21.7	22.2	22.5	23.1	23.5	23.9	24.3	24.8	25.2
convex curvature change [10^{-5} m^{-1}]	0	1.81	2.87	2.57	3.17	4.3	5.09	5.17	5.69	6.36
rms slope error [µrad]	0.55	0.70	0.97	0.87	1.00	1.27	1.41	1.47	1.60	1.74
required defocus compensation [mm]	0.00	0.10	0.17	0.20	0.25	0.26	0.28	0.30	0.35	0.40
rms slope error after defocus compensation [µrad]	0.55	0.56	0.68	0.65	0.71	0.78	0.76	0.87	0.83	0.87

Figures 9 and 10 present the data of the first two rows in Table 2 in a graphical form. The linear dependences in Figs. 9 and 10 can be predicted based on the linearity of the temperature dependence of thermal expansion and on the linear character of the bending equation [7,15]:

$$\frac{d^2y}{d^2x} = C_A g_A(x) + C_B g_B(x), \qquad (2)$$

where

$$g_A(x) \equiv \left(\frac{1}{2} - \frac{x}{L}\right)\frac{1}{E\,I(x)} \quad \text{and} \quad g_B(x) \equiv \left(\frac{1}{2} + \frac{x}{L}\right)\frac{1}{E\,I(x)}, \tag{3}$$

and C_A and C_A are the bending couples, E is Young's modulus, and $I(x)$ is the moment of inertia of the substrate cross section. The best-fit linear approximations

$$\delta Cur = -1.6(T - 21.0)\times 10^{-5}\,\mathrm{m}^{-1} \quad \text{and} \tag{4a}$$

$$\delta Slope = [0.28(T - 21.0) + 0.55]\ \mu\mathrm{rad\ (rms)} \tag{4b}$$

are shown in Figs. 9 and 10 with the dashed lines.

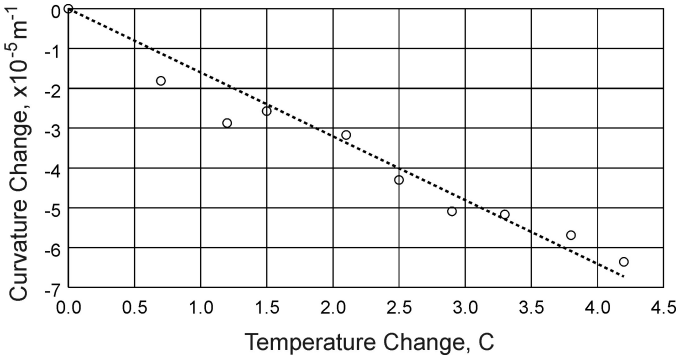

Fig. 9. The mirror curvature change as a function of the container temperature. The dashed line shows a linear fit.

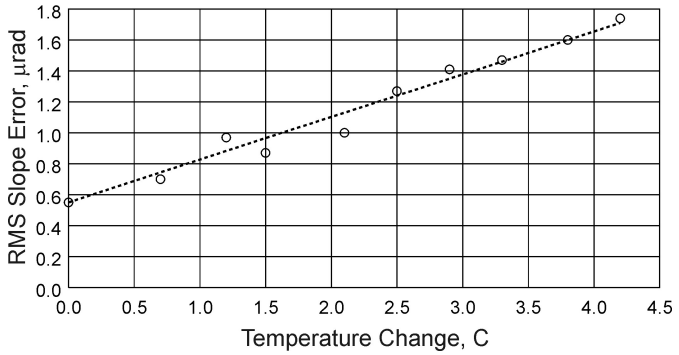

Fig. 10. The rms slope error of the mirror surface shape as a function of the container temperature. The dashed line shows a linear fit.

In summary, without thermal stabilization, we observe a high sensitivity of the mirror shape to the ambient temperature. Temperature variations by a few degrees causes several micro-radians surface slope error: a magnitude that would be unacceptable for most applications. The following section shows that the temperature sensitivity problem can be solved using an active temperature stabilization of the mirror body based on a Peltier element.

7. Effectiveness of the mirror temperature stabilization

To investigate the effectiveness of the thermally-stabilized KB mirror holder, a series of LTP measurements were conducted, in a similar manner to those described in the

previous section. Using a dedicated Thorlabs^{TM} temperature controller, the mirror body temperature was set to 21.3 C.

Figure 11 summarizes the slope measurements conducted at three different stable ambient temperatures. This time, while the temperature within the container increased, the slope error profile of the mirror remains unchanged. The observable increase of the random error is an artifact of the measurements associated with air convection along the LTP optical path [34]. The larger temperature inside the container, the stronger is the perturbation of the LTP light beam direction due to air convection.

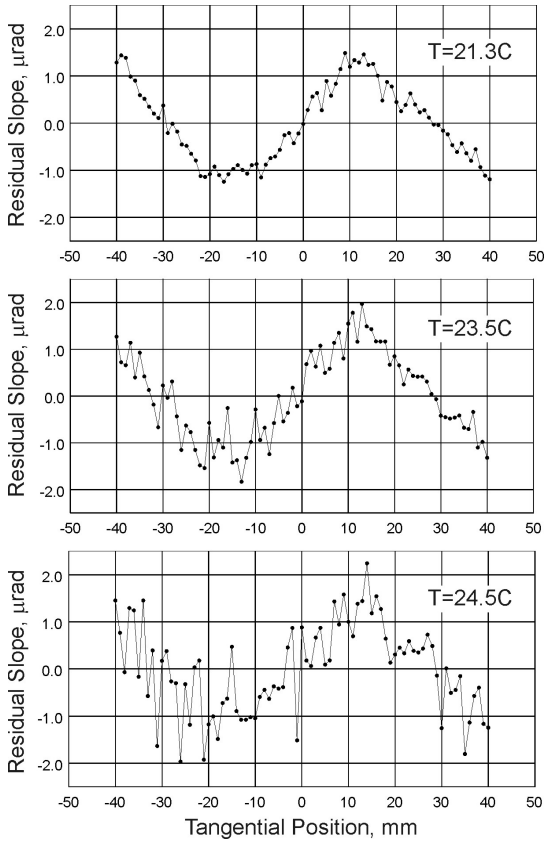

Fig. 11. The residual variation of the mirror tangential slope measured at different temperatures inside the container without adjusting the bending couplings. The temperature controller attached to the bender body was set to constant 21.3ºC. The traces correspond to the sagittal center of the mirror. Unlike the previous case, with no active temperature stabilization (Fig. 7), the mirror figure remains constant. The increase of the random noise is due to the air convection that becomes stronger at higher temperature inside the container.

Figure 12 shows a surface slope change at T = 24.5 C, relative to the 21.3 C slope trace. Compared with the earlier results, in Fig. 8, the measurements with the thermally-stabilized mirror assembly show a significant suppression of the shape change effects.

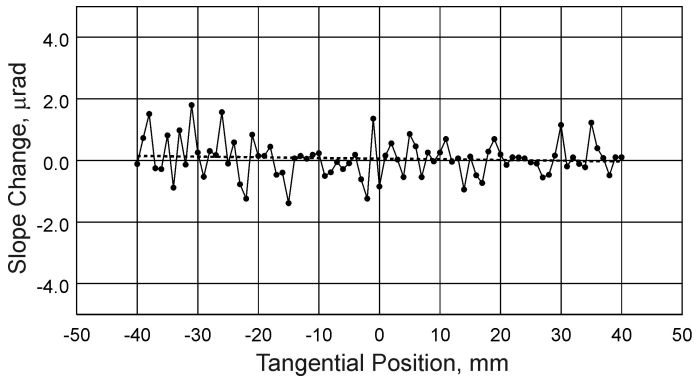

Fig. 12. Temperature-induced surface slope change with a 3.2 C (24.5 C – 21.3 C) increase in the ambient temperature. The dashed line is a linear fit. Unlike the previous case without temperature stabilization (Fig. 8), here slope changes are not detectable within a measurement uncertainty of 3 nrad/mm that corresponds to a radius of curvature above 300 km.

8. Conclusions and Discussion

We have demonstrated that active temperature stabilization, based on a Peltier element attached directly to the body of an elliptically bent KB mirror, provides mirror surface shape stability under several degrees of ambient temperature change. The design and the materials used in the mirror assembly have been carefully optimized to provide high heat conductance between the mirror body and its substrate.

Using a specially fabricated test mirror placed inside a temperature-controlled container, we investigated the thermal sensitivity of the mirror surface profile with and without active control of the mirror holder temperature. Without thermal stabilization, the rms variation of the mirror slope, measured with an LTP across an 80 mm clear aperture, changed by more than 4 µrad, with an equivalent curvature change of 6.36 $10^{-5}m^{-1}$ under a 4.2 C temperature increase. However, with active thermal stabilization, in the presence of a 3.2 C temperature increase, the mirror slope did not noticeably change, within our measurement uncertainty, which is below 0.1 µrad.

The KB mirror, described throughout this work, is intended for use as a test x-ray optic at ALS beamline 5.3.1. The beamline endstation, now under construction, is dedicated to at-wavelength, in situ metrology of x-ray optics [31,32]. The test mirror's measured residual surface figure error of 0.5 µrad (rms) is relatively large when compared with the mirrors of the same design currently in use at the ALS beamline 10.3.2 and 12.3.2. We attribute this to the fact that this is an older, spare substrate with a significant sagittal width and/or thickness error. Contributions to the figure error may also come from the residual stress due to the imperfections of the mirror assembly. We are working on a upgrade of the mirror design that would allow us to significantly reduce the residual stress.

For the purposes of this investigation (separate from a beamline focusing application), the presence of the figure error is useful for distinguishing real changes of the mirror shape from measurement errors. Similarly, when using the mirror for testing at-wavelength metrology techniques, the known, residual figure error is a useful peculiarity that should be observable in the course of the metrology.

9. Acknowledgements

This work was supported by the Director, Office of Science, of the U.S. Department of Energy under Contract No. DE-AC02-05CH11231.

DISCLAIMER

References

1. L. Assoufid, O. Hignette, M. Howells, S. Irick, H. Lammert, P. Takacs, *Future metrology needs for synchrotron radiation grazing-incidence* optics, Nucl. Instrum. and Meth. A **467-468**, 267–70 (2001).
2. A Erko, M. Idir, T. Krist, A. G. Michette (Eds), *Modern developments in X-ray and Neutral Optics*, Springer, Berlin, 2007.
3. P. Kirkpatrick and A. V. Baez, *Formation of Optical Images by X-Rays,* J. Opt. Soc. Am. **38** (9), 766–74 (1948).
4. C. Liu, L. Assoufid, R. Conley, A. T. Macrander, G. E. Ice, J. Z. Tischler, *Profile coating and its application for Kirkpatrick-Baez mirrors*, Opt. Eng., **42** (12), 3622–8 (2003).
5. H. Yumoto, H. Mimura, S. Matsuyama, H. Hara, K. Yamamura,Y. Sano, K. Ueno, *Fabrication of elliptically figured mirror for focusing hard x rays to size less than 50 nm*, Rev. Sci. Instrum. **76**, 063708 (2005).
6. F. Siewert, H. Lammert, T. Noll, T.; T. Schlegel, T. Zeschke, T. Hansel, A. Nickel, A. Schindler, B. Grubert, C. Schlewitt, *Advanced metrology, an essential support for the surface finishing of high performance X-ray optics*, Proc. SPIE **5921**, 592101-1-11 (2005).
7. M. R. Howells, D. Cambie, R. M. Duarte, S. Irick, A. A. MacDowell, H. A. Padmore, T. R. Renner, S. Rah, R. Sandler, *Theory and practice of elliptically bend x-ray mirrors,* Opt. Eng. **39** (10) 27-48-2762 (2000).
8. P. Z. Takacs, "X-Ray Mirror Metrology," in M. Bass (Ed.), *Handbook of Optics*, third ed., vol. V, chapter 46, McGraw-Hill Publishing Company, New York (2009).

9. F. Siewert, H. Lammert, T. Zeschke, "*The Nanometer Optical Component Measuring Machine*;" in: A Erko, M. Idir, T. Krist, A. G. Michette (Eds), Modern Developments in X-ray and Neutron Optics, Springer, Berlin 2008.

10. Ralf D. Geckeler, "*ESAD Shearing Deflectometry: Potentials for Synchrotron Beamline Metrology,*" Proc. SPIE, **6317**, 63171H-1-13 (2006).

11. T. Kimura, H. Ohashi, Hidekazu Mimura, D. Yamakawa, H. Yumoto, S. Matsuyama, T. Tsumura, H. Okada, T. Masunaga, Y. Senba, S.Goto, T. Ishikawa, K. Yamauchi, *A stitching figure profiler of large X-ray mirrors using RADSI for sub-aperture data acquisition,* Nucl. Instr. and Meth. A, doi: 10.1016/j.nima.2009.11.014.

12. Jonathan L. Kirschman, Edward E. Domning, Wayne R. McKinney, Gregory Y. Morrison, Brian V. Smith, and Valeriy V. Yashchuk, *Performance of the upgraded LTP-II at the ALS Optical Metrology Laboratory,* Proc. SPIE **7077**, 7077-10-1/12 (2008).

13. V. V. Yashchuk, S. Barber, E. E. Domning, J. L. Kirschman, G. Y. Morrison, B. V. Smith, F. Siewert, T. Zeschke, R. Geckeler, A. Just, *Sub-microradian Surface Slope Metrology with the ALS Developmental Long Trace Profiler,* Nucl. Instr. and Meth. A, doi: 10.1016/j.nima.2009.10.175.

14. W. R. McKinney, S. C. Irick, J. L. Kirschman, A. A. MacDowell, A. Warwick, V. V. Yashchuk, *New Procedure for the Adjustment of Elliptically Bent Mirrors with the Long Trace profiler,* Proc. of SPIE **6704**, 67040G, (2007).

15. W. R. McKinney, S. C. Irick, J. L. Kirschman, A. A. MacDowell, A. Warwick, V. V. Yashchuk, *Optimal tuning and calibration of bendabale mirrors with with slope measuring profilers,* Opt. Eng. **48** (8), 083601 (2009).

16. S. Mourikis, W. Jark, E. E. Koch, V. Saile, *Surface temperature and distortion of optical elements exposed to high power synchrotron radiation beams,* Rev. Sci. Instrum. **60** (7), 1474–8 (1989).

17. T. Warwick, S. Sharma, *Thermal effects and mirror surface figure requirements for a diagnostic beamline at the Advanced Light Source,* Nucl. Instr. and Meth. A **319**, 185–7 (1992).

18. N. Kihara, K. Mashima, S. Miura, A. Miyaji, K. Wakamiya, S. Ichikawa, *Thermal and deformation analyses of side-cooled monochromator mirrors for the Spring-8/Figure-8 soft x-ray undulator,* J. Synchrotron Rad. **5**, 811–3 (1998).

19. K. Freund, *Challenges for synchrotron x-ray optics,* Proc. SPIE **4782**, 1–12 (2002).

20. R. K. Smither, W. Lee, A. Macrander, S. Rogers, *Recent experiments with liquid gallium cooling of crystal diffraction optics,* Rev. Sci. Instrum. **63** (2) 1746–54 (1992).

21. M. R. Howells, *Some fundamentals of cooled mirrors for synchrotron radiation beam lines,* Opt. Eng. **35** (4), 1187–97 (1996).

22. R. Beguiristain, J.H. Underwood, M. Koike, P. Batson, H. Medecki, S. Rekawa, K. Jackson, D. Atwood, *Characterization of thermal distortion effects on beamline optics for EUV interferometry and soft X-ray microscopy,* Rev. Sci. Instrum. **67** (9), 1–9 (1996).

23. K. A. Goldberg, R. Beguiristain, J. Bokor, H. Medecki, K. Jackson, D. T. Attwood, G. E. Sommargren, J. P. Spallas, R. Hostetler, *At-wavelength testing of optics for EUV*, Proc. SPIE **2437**, 347–54 (1995).

24. S. Qian, W. Jark, P. Z. Takacs, K. J. Randall, W. Yun, *In situ surface profiler for high heat load mirror measurement*, Opt. Eng. **34** (2), 396–402 (1995).

25. S. Qian, W. Jark, G. Sostero, A. Gambitta, F. Mazzolini, A. Savoia, *Precise measuring method for detecting the in situ distortion profile of a high-heat-load mirror for synchrotron radiation by use of a pentaprism long trace profiler*, Appl. Opt. **36** (16), 3769–75 (1997).

26. P. Z. Takacs, S. Qian, K. J. Randall, W. B. Yun, H. Li, *Mirror distortion measurements with an in-situ LTP*, Proc. SPIE **3447**, 117–24 (1998).

27. Hignette, A. Freund, E. Chinchio, *Incoherent x-ray mirror surface metrology*, Proc. SPIE **3152**, 188–99 (1997).

28. P. Revesz, A. Kazimirov, I. Bazarov, *In situ visualization of thermal distortions of synchrotron radiation optics*, Nucl. Instr. and Meth. A **576**, 422–9 (2007).

29. T. Kimura, S. Handa, H. Mimura, H. Yumoto, D. Yamakawa, S.Matsuyama, Y. Sano, K. Tamasaku, Y. Nishino, M. Yabashi, T. Ishikawa, K. Yamauchi, *Development of adaptive mirror for wavefront correction of hard X-ray nanobeam*, Proc. SPIE **7077**, 707709-1-8 (2008).

30. M. Kunz, N. Tamura, K. Chen, A. A. MacDowel, R. S. Celestre, M. M. Church, S. Fakra, E. E. Domning, J. M. Glossinger, J. Kirschman, G. Y. Morrison, D. W. Plate, B. V. Smith, T. Warwick, V. V. Yashchuk, H. A. Padmore, and E. Ustundag, *A dedicated superbend x-ray microdiffraction beamline for materials-, geo- and environmental sciences at the Advanced Light Source*, Rev. Sci. Instrum. **80**(8), 035108/1-10 (2009).

31. S.Yuan, K. Goldberg, V. V. Yashchuk, R. Celestre, T. Warwick, W. R. McKinney, G. Morrison, S. B. Rekawa, I. Mochi, H. A. Padmore, *At-wavelength and optical metrology of bendable x-ray optics for nanofocusing at the ALS*, Extended Abstract in the Digest of the OSA Optics and Photonics Congress: Frontiers in Optics 2009, Laser Science XXV, Special Symposium on Optics for Imaging at the Nanoscale and Beyond (San Jose, California, USA, October 11-15, 2009).

32. S. Yuan, M. Church , R. Celestre, G. Morrison, W. McKinney, T. Warwick, K. Goldberg, V. Yashchuk, *Surface slope metrology and interferometric wave front measurements on deformable soft x-ray mirrors performed in the laboratory and in-situ at-wavelength*, The Tenth International Conference on Synchrotron Radiation Instrumentation (Melbourne, Victoria, Australia. September 27–October 2, 2009).

33. V. V. Yashchuk, *Optimal Measurement Strategies for Effective Suppression of Drift Errors*, Rev. Sci. Instrum. **80**, 115101-1-10 (2009).

34. V. V. Yashchuk, S. C. Irick, A. A. MacDowell, W. R. McKinney, P. Z. Takacs, *Air convection noise of pencil-beam interferometer for long-trace profiler*, Proc. SPIE **6317**, 631713-1-12 (2006).